Determination of the Melting and Solidification Characteristics of Solders Using Differential Scanning Calorimetry

SINN-WEN CHEN, CHAO-CHING LIN and CHIH-MING CHEN

Differential scanning calorimetry (DSC) is used in the present study to determine the onset temperature of phase transformation and the enthalpy of fusion of various solder alloys. The solders studied are Sn-Pb, Sn-Bi, Ag-Sn, In-Ag, and Sn-Pb-Bi alloys. Very notable undercooling, such as 35 °C, is observed in the solidification process; however, a superheating effect is not as significant in the heating process. Besides the direct measurements of reaction temperature and heat of fusion, the fraction solid *vs* temperature has also been determined using a DSC coupled with a mathematical-model method. The heating and cooling curves of the solders are first determined using DSC. By mathematically modeling the heat transfer of the DSC cells, the heat evolution and absorption can be calculated, and then the melting and solidification curves of the solder alloys are determined. The three ternary alloys, Sn-35 wt pct Pb-10 wt pct Bi, Sn-45 wt pct Pb-10 wt pct Bi, and Sn-55 wt pct Pb-10 wt pct Bi, displayed similar DSC cooling curves, which had three reaction peaks. However, the solid fractions of the three alloys at the same temperature in the semisolid state, which had been determined quantitatively using the DSC coupled with a mathematical method, were different, and their primary solidification phases were also different.

I. INTRODUCTION

Soldering, a joining process of two substrates, is a very important technique in the packaging of electronic products.[1,2] Wave soldering and reflow soldering are the two most common soldering techniques used in the electronic industry, and there is a trend of an increasing demand for the reflow process. This trend has been strongly connected with the change from pin-through-hole technology to surface-mount technology in module-to-board assembling. Surface-mount devices are placed on solders printed on the printed circuit board, and the board is then passed through a reflow furnace. Following the temperature profile of the furnace, the solders are first heated up, then become molten, react with the substrates; cool down, and solidify. The temperature profile of the reflow furnace is a key process parameter for obtaining a good assembly. Insufficient heating can result in nonwetting at the solder joint, whereas excessive heating introduces enhanced interfacial reactions and possible reliability problems. The knowledge of melting and solidification characteristics of solders is valuable in the selection of the temperature profile of the reflow furnace.

Differential scanning calorimetry (DSC) is used in the present study to determine the melting and solidification characteristics, such as the onset temperatures of phase transformation, the enthalpy of fusion, and the fraction solid *vs* temperature of solders. Various techniques can be applied to the determination of the melting and solidification curves, which are the relationships of the fraction solid *vs* temperature of the heating and cooling processes.[3–12] The most direct method is by quenching the specimen during processing, and then analyzing the amount of solid prior to quenching using image analysis. Difficulties encountered in using this method, such as quenchability and segregation, have been discussed previously.[9,10,11] A technique has been successfully applied to various alloys using differential thermal analysis (DTA) to determine the cooling curves of alloys and then calculating the solidification curves based on the determined cooling curves with heat-transfer models.[9,10,11] The DSC technique is similar to DTA, but instead of measuring the temperature difference between the reference cell and the sample cell, DSC measures the energy input difference between the two cells.[12] The DTA method requires the conversion of the measured temperature difference to the energy difference in the solidification-curve calculation. Since the DSC measures the energy difference directly, it is likely to achieve an improved accuracy over DTA in the determination of melting and solidification curves.

The Sn-Pb solders, especially the eutectic Sn-37 wt pct Pb alloy, are the most often used solders. The Sn-Pb solders have good solderability and good mechanical properties. It has been reported that 10^{12} solder joints are produced annually in the electronic industry,[1] and most of them are made with Sn-Pb solders. However, because of environmental and health concerns, Pb-free solders have been actively under investigation.[13–16] Another trend in solder development is the search for alloys of lower melting temperatures to avoid the popcorn-effect problem, which is commonly encountered in the thin plastic packages.[17,18] The Sn-Bi, Ag-Sn, In-Ag, and Sn-Pb-Bi alloys are among the most intensively investigated. The DSC technique is used in this study to determine the melting and solidification characteristics of the solder alloys of the following compositions: Sn-37 wt pct Pb, Sn-58 wt pct Bi, Ag-96.5 wt pct Sn, In-20 wt pct Ag, In-15 wt pct Ag, In-10 wt pct Ag, Sn-55 wt pct Pb-10 wt pct Bi, Sn-45 wt pct Pb-10 wt pct Bi, Sn-35 wt pct Pb-10 wt pct Bi, Sn-43 wt pct Pb-14 wt pct Bi, and Sn-42 wt pct Pb-8 wt pct Bi.

SINN-WEN CHEN, Professor, and CHAO-CHING LIN and CHIH-MING CHEN, Graduate Students, are with the Department of Chemical Engineering, National Tsing-Hua University, Hsin-Chu, Taiwan 30043, Republic of China.

Manuscript submitted October 17, 1997.

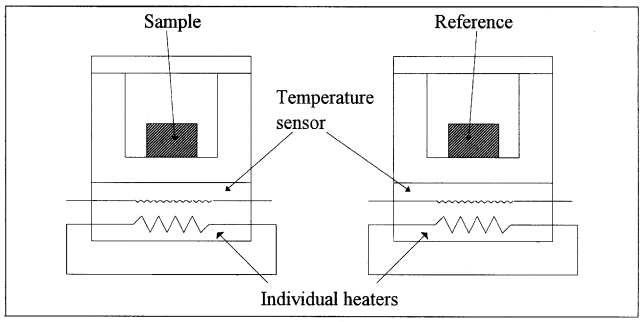

Fig. 1—A schematic diagram of DSC.

II. EXPERIMENTAL PROCEDURES

The solders were prepared from elements with purity higher than 99.99 wt pct. Proper amounts of the constituent elements were weighed using an electronic balance, sealed in a quartz tube under 10^{-3} torr vacuum, melted at 500 °C in the furnace for 3 hours, and then quenched in water. The chemical homogeneity of the solder alloys was examined using inductively coupled plasma spectroscopy (ICP).

A PERKIN-ELMER* DSC was used in the present study. Ten milligrams of the solder alloy were cut from the alloy ingot prepared using the aforementioned method, and the solder specimen was then contained in a DSC aluminum holder. A thin layer of alumina powder was placed between the aluminum holder and the solder. It was observed that without the alumina layer, the solder adhered to the aluminum holder after the thermal analysis, and the alumina-powder layer eliminated the sticking problem.

The aluminum holder that contained the solder specimen was placed in the sample cell in the DSC, while an empty aluminum holder was placed in the reference cell. The sample was first preheated at 120 °C for 2 hours, then heated to about 50 °C higher than the melting point of the solder alloy at a constant heating rate, held isothermally for 10 minutes, and then cooled down to room temperature at a constant cooling rate. The scanning rates examined were 10 °C/min and 1.25 °C/min.

*PERKIN-EIMER is a trademark of Perkin-Elmer Physical Electronics, Eden Prairie, MN.

III. MATHEMATICAL MODELING OF DSC CURVES

A schematic diagram of the DSC equipment is shown in Figure 1. The sample and reference cells both contain a pan attached with a thermocouple and heating elements. The two cells are maintained at the same temperature, T_p, and are controlled by the balance of the thermal energy added to the cells from the heating elements and the heat flux lost to the surroundings. The temperature of these two cells, T_p, and the difference of the rates of energy input to the respective heating elements are monitored and recorded in the DSC. In the event that a phase transition occurs in the sample, latent heat is evolved or absorbed. The energy input to the sample cell is changed to compensate the phase-transformation energy in order to maintain the two cells at the same temperature. A typical DSC thermogram is shown in Figure 2; the Sn-37 wt pct Pb solder melts at 183 °C and the enthalpy of fusion is 45.2 J/g.

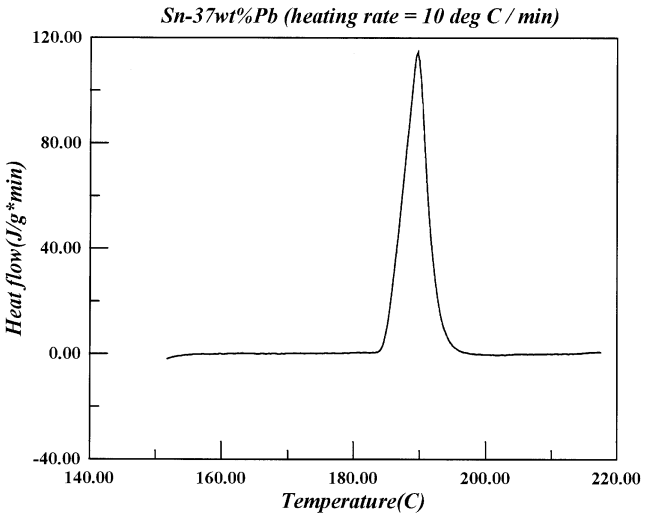

Fig. 2—The DSC heating curve of the Sn-37 wt pct Pb at the heating rate of 10 °C/min.

Gray[19] assumes that the temperatures in the sample container (including the samples) are uniform and that the major heat-transfer resistance is between the sample holder and the sample container, and similar assumptions are also applied to the reference cell. Based on these assumptions, and on the principle of energy conservation, the following equations can be derived for the sample and the reference cells, respectively:

$$C_s \frac{dT_s}{dt} = \frac{dq_s}{dt} + \frac{dh}{dt} \quad [1a]$$

$$C_r \frac{dT_r}{dt} = \frac{dq_r}{dt} \quad [1b]$$

where T is the temperature, t the time, C the heat capacity of the cell, dq/dt the rate of energy input to the sample container, and dh/dt the rate of heat generation of the sample. The subscripts s and r denote the sample cell and the reference cell, respectively. The rate of energy input can be described by Newton's law, as follows:

$$\frac{dq_s}{dt} = \frac{(T_p - T_s)}{R_s} \quad [2a]$$

$$\frac{dq_r}{dt} = \frac{(T_p - T_r)}{R_r} \quad [2b]$$

where R is the heat-transfer resistance between the container and the holder and T_p is the temperature of the pan, which is identical in the sample and the reference cells. From the first derivative of Eq. [2a], the following equation can be obtained:

$$\frac{dT_s}{dt} = \frac{dT_p}{dt} - R_s \frac{d^2q_s}{dt^2} \quad [3a]$$

Since there is no phase change in the reference cell and dT_p/dt is constant, the following is further assumed:

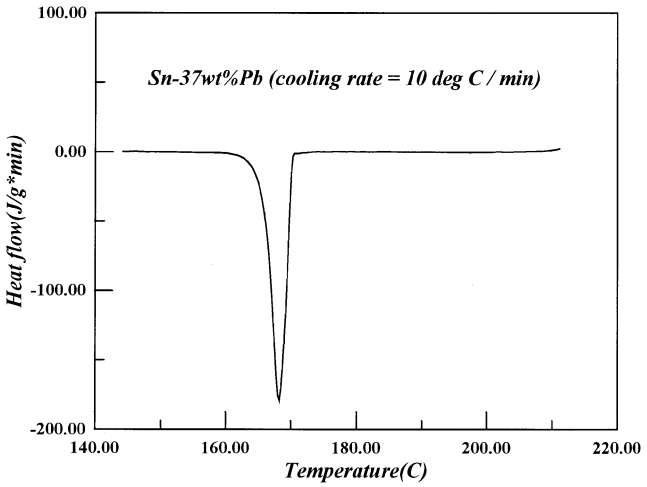

Fig. 3—The DSC cooling curve of the Sn-37 wt pct Pb at the cooling rate of 10 °C/min.

$$\frac{dT_r}{dt} = \frac{dT_p}{dt} \qquad [3b]$$

$$\frac{d^2q_r}{dt^2} = 0 \qquad [3c]$$

The following equation can then be derived from Eqs. [1] and [3].

$$\frac{dh}{dt} = -\frac{dq}{dt} + (C_s - C_r)\frac{dT_p}{dt} - R_sC_s\frac{d^2q}{dt^2} \qquad [4a]$$

The term $q = (q_s - q_r)$ is the difference in the energy input between the sample cell and the reference cell, and is measured in the DSC experiment. The term $(C_s - C_r)\ dT_p/dt$, which is the deviation from the baseline, is usually eliminated in the DSC calibration procedures, and thus Eq. [4a] can be rewritten as follows:

$$\frac{dh}{dt} = -\frac{dq}{dt} - R_sC_s\frac{d^2q}{dt^2} \qquad [4b]$$

Equation [4b] can be written in the finite-difference form and solved numerically.

$$\frac{\Delta h}{\Delta t} = -\frac{\Delta q}{\Delta t} - R_sC_s\left[\frac{\frac{\Delta q}{\Delta t}_{(t+\Delta t)} - \frac{\Delta q}{\Delta t}_{(t)}}{\Delta t}\right] \qquad [4c]$$

As mentioned previously, T_p and dq/dt are measured in the DSC experiment. Since the scanning rate, dT_p/dt, is constant, Δt at a specific T_p is thus known. The term R_sC_s is a system parameter that must be determined. The relationship between the latent heat evolution, h, and the reaction time, t, can then be obtained from the solution of Eq. [4c] based on the knowledge of the DSC thermogram and the determined R_sC_s. The fraction of solidified (or molten) phase during solidification (or melting) can be determined, if it is further assumed that the amount of latent heat evolution is directly proportional to the amount of solidified (or molten) solder. The value of R_sC_s can be determined by two different methods: the trial-and-error method or use of the after-reaction curve. The principle of the trial-and-error method is that the fraction of phase transformation is 100 pct at the end of the phase transformation. By giving an initial value to R_sC_s, the fraction of phase transformation can be calculated, and the true value of the R_sC_s can thus be determined by an iteration procedure. The principle of the other approach is that at the end of the reaction, there is no further heat evolution (or absorption), and the value of the dh/dt in Eq. [4b] is zero. Equation [4b] is reduced to the following:

$$\frac{dq}{dt} = R_sC_s\frac{d^2q}{dt^2} \qquad [4d]$$

With the initial conditions that the end of the reaction is the beginning of the after-reaction, *i.e.*, $t' = (t - t_{max}) = 0$ and $(\frac{dq}{dt})_{t'=0} = (dq/dt)_{max}$, Eq. [4d] can be solved and the following equation is obtained:

$$\left(\frac{dq}{dt}\right) = \left(\frac{dq}{dt}\right)_{max} e^{-\frac{t'}{R_sC_s}} \qquad [5]$$

It is clear that the after-reaction curve is an exponential curve, and the value of R_SC_S can be determined using a curve-fitting technique. In this study, the value determined from the after-reaction curve is used as the initial value for the trial-and-error method. It has been found that the values of R_SC_S determined using these two different methods are similar.

IV. RESULTS AND DISCUSSION

The DSC heating curve of the most commonly used solder, Sn-37 wt pct Pb alloy, at the heating rate of 10 °C/min, is shown in Figure 2. The eutectic reaction began at 183 °C, which was the onset of the reaction peak of the heating curve, and the alloy became completely molten at 190 °C, which was the temperature that the reaction peak reached its maximum. The onset temperature is identical to the equilibrium eutectic temperature of 183 °C,[20] which indicates that superheating effects are insignificant for the melting of the Sn-37 wt pct Pb alloy at the heating rate of 10 °C/min. Similar to most alloys, undercooling during solidification of the Sn-37 wt pct Pb alloy is much more pronounced than superheating in the melting. The DSC cooling curve of the Sn-37 wt pct Pb alloy at the cooling rate of 10 °C/min is shown in Figure 3. The beginning of the solidification is at 172 °C, and the undercooling is at 11 °C.

Based on the DSC curve of Sn-37 wt pct Pb alloy determined at a 1.25 °C/min heating rate, the eutectic reaction began at 184 °C and was completed at 187 °C. The melting range determined at the heating rate of 1.25 °C/min was 3 °C and was narrower than the 7 °C determined for 10 °C/min. Since Sn-37/wt pct Pb is a eutectic alloy, its melting reaction should occur at a constant temperature. The melting range observed in the DSC heating curve can result from the temperature inhomogeneity within the DSC sample container (and the sample) itself. This is expected, since a slower scanning rate reduces the temperature inhomogeneity, and thus the observed temperature range of melting decreases as well. Another possibility for this phenomenon is that Sn-37 wt pct Pb is not a eutectic alloy. Although the Sn-37 wt pct Pb alloy is considered a eutectic alloy com-

Table I. Summary of DSC Results

Composition (Pct)	Scaning Rate (°C/min)	Reaction Temperature(s) (°C)			Enthalpy of Fusion (J/g)
Sn-3.5 wt pct Ag	10	222	—	—	68.2
Sn-3.5 wt pct Ag	−10	186	—	—	−65.6
Sn-3.5 wt pct Ag	1.25	218	—	—	66.4
Sn-3.5 wt pct Ag	−1.25	200	—	—	−64.6
Sn-58 wt pct Bi	10	139	—	—	43.2
Sn-58 wt pct Bi	−10	123	—	—	−42.7
Sn-58 wt pct Bi	1.25	138	—	—	49.1
Sn-58 wt pct Bi	−1.25	131	—	—	−49.8
Sn-37 wt pct Pb	10	183	—	—	45.2
Sn-37 wt pct Pb	−10	172	—	—	−44.
Sn-37 wt pct Pb	1.25	184	—	—	48.2
Sn-37 wt pct Pb	−1.25	172	—	—	−49.1
In-10 wt pct Ag	10	142	168	—	38.3
In-10 wt pct Ag	−10	233	136	—	−37.9
In-10 wt pct Ag	1.25	143	167	—	41.6
In-10 wt pct Ag	−1.25	240	140	—	−43.0
In-15 wt pct Ag	10	142	167	—	42.5
In-15 wt pct Ag	−10	279	136	—	−40.8
In-15 wt pct Ag	1.25	144	169	—	41.4
In-15 wt pct Ag	−1.25	288	140	—	−43.1
In-20 wt pct Ag	10	143	168	343	37.4
In-20 wt pct Ag	−10	323	136	—	−41.4
In-20 wt pct Ag	1.25	144	169	—	39.4
In-20 wt pct Ag	−1.25	329	143	—	−43.0
Sn-42 wt pct Pb-8 wt pct Bi	10	154	—	—	38.0
Sn-42 wt pct Pb-8 wt pct Bi	−10	171	162	128	−41.6
Sn-42 wt pct Pb-8 wt pct Bi	1.25	155	163	—	39.0
Sn-42 wt pct Pb-8 wt pct Bi	−1.25	179	171	—	−37.9
Sn-43 wt pct Pb-14 wt pct Bi	10	134	140	—	38.4
Sn-43 wt pct Pb-14 wt pct Bi	−10	160	151	128	−36.3
Sn-43 wt pct Pb-14 wt pct Bi	1.25	135	137	168	35.6
Sn-43 wt pct Pb-14 wt pct Bi	−1.25	166	159	134	−35.8
Sn-35 wt pct Pb-10 wt pct Bi	10	135	142	—	42.7
Sn-35 wt pct Pb-10 wt pct Bi	−10	147	142	128	−43.5
Sn-35 wt pct Pb-10 wt pct Bi	1.25	135	142	—	46.0
Sn-35 wt pct Pb-10 wt pct Bi	−1.25	164	134	—	−45.3
Sn-45 wt pct Pb-10 wt pct Bi	10	143	150	—	38.4
Sn-45 wt pct Pb-10 wt pct Bi	−10	176	160	130	−40.5
Sn-45 wt pct Pb-10 wt pct Bi	1.25	136	142	—	44.0
Sn-45 wt pct Pb-10 wt pct Bi	−1.25	179	162	—	−44.3
Sn-55 wt pct Pb-10 wt pct Bi	10	121	153	175	30.7
Sn-55 wt pct Pb-10 wt pct Bi	−10	197	153	128	−32.2
Sn-55 wt pct Pb-10 wt pct Bi	1.25	135	141	171	34.2
Sn-55 wt pct Pb-10 wt pct Bi	−1.25	202	163	134	−35.0

mercially, the phase diagram assessed by Karakaya and Thompson[20] indicates that the eutectic composition is Sn-38.1 wt pct Pb, and that the Sn-37 wt pct Pb is a hypoeutectic alloy rather than a eutectic alloy.

The enthalpy of fusion can be determined by computing the peak area of the DSC curve. As listed in Table I, the values of the enthalpy of fusion of the Sn-37 wt pct Pb alloy determined from the heating curves at the heating rates of 10 °C/min and 1.25 °C/min are 45.1 and 48.2 J/g, respectively. The variation of the fusion enthalpy measurement can be caused by various factors. The sample weight of the DSC specimen is about 10 mg, and the uncertainty of the measurement is about 2 pct Other factors, such as uncertainties in the determination of the baseline, *i.e.*, the onset and completion temperatures of the peak in the DSC curves, can also contribute to the variation of enthalpy measurement.

Similar results were found for the other eutectic solder alloys, and are summarized in Table I. The onset of the eutectic reaction of the Sn-58 wt pct Bi alloy was 139 °C at 10 °C/min heating rate and 138 °C at 1.25 °C/min heating rate. With the experimental uncertainty of the DSC measurement taken into consideration, these results are in good agreement with the literature value[21] of 139 °C. Undercooling of 16 °C and 8 °C was observed from the cooling curves determined at 10 °C/min and 1.25 °C/min cooling rates, respectively. For the Sn-3.5 wt pct Ag alloy, the eutectic temperatures determined from the heating curves were 222 °C and 218 °C, which were close to the literature value of 221 °C.[22] Very pronounced undercooling phenomena were found for the Sn-3.5 wt pct Ag alloy. These undercoolings were 35 °C and 21 °C for the solidification at 10 °C/min and 1.25 °C/min cooling rates, respectively.

Three reactions are found in the DSC heating curve of a

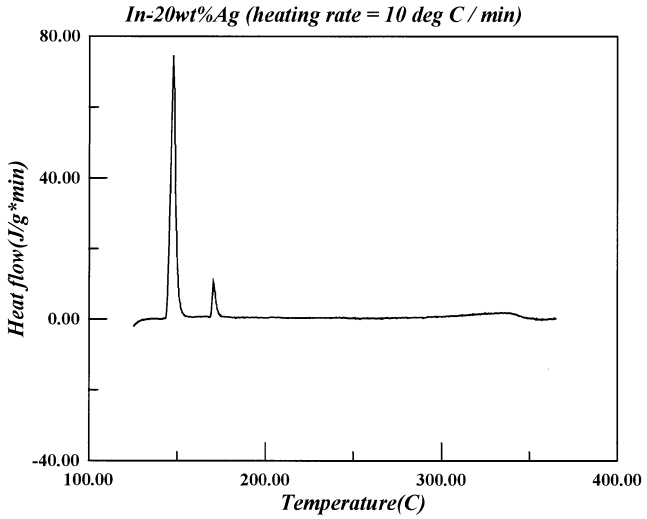

Fig. 4—The DSC heating curve of the In-20 wt pct Ag at the heating rate of 10 °C/min.

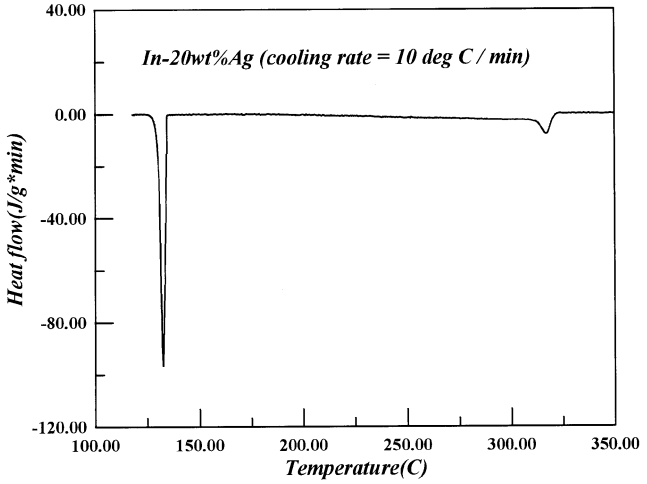

Fig. 5—The DSC cooling curve of the In-20 wt pct Ag at the cooling rate of 10 °C/min.

noneutectic binary In-20 wt pct Ag solder alloy (Figure 4). According to the In-Ag equilibrium phase diagram,[23] the heating of the In-20 wt pct Ag alloy should encounter a eutectic reaction, a peritectic reaction, a metatectic reaction, and the liquidus curve. The largest peak, which has an onset at 143 °C, corresponds to the eutectic reaction, and the smaller peak at 168 °C results from the peritectic reaction. The alloy became completely molten at a temperature higher than the liquidus temperature at 343 °C, as can be determined from the baseline change in Figure 4. The metatectic reaction, which corresponds to the formation of ζ phase in the heating process, cannot be found in Figure 4. The ζ phase does not exist in the In-20 wt pct Ag alloy at room temperature. During the heating process, the $AgIn_2$ phase decomposes and forms the ζ phase. It is likely that the transformation rate of this reaction, $AgIn_2 = L + \zeta$, is not fast enough, and only a small amount of ζ phase is formed, such that the metatectic reaction $\zeta = L + \gamma$ cannot be detected. Figure 5 shows the DSC cooling curve of the In-20 wt pct Ag alloy. The primary solid formation first occurred at 323 °C. It is also noticed that the liquidus temperature can be observed more clearly in the cooling curve than in the heating curve. A similar phenomenon was found for the In-15 wt pct Ag and the In-10 wt pct Ag alloys. In fact, this phenomenon is very common for most alloys and primarily results from the effect of undercooling. In the heating scan, when the temperature is close to that of the liquidus surface, alloy melts gradually with increasing temperature and there is no sudden change. However, in the cooling scan, when the temperature of the melt just passes that of the liquidus temperature, there is no solid formation, because of the effect of undercooling. As soon as a certain degree of undercooling is reached and the solid has been nucleated, there is a drive of the formation of a certain amount of solid, depending upon the amount of undercooling. The thrust of heat release contributes to the enhancement of the liquidus temperature peak. Thus, the reaction mechanism can usually be observed more clearly in the cooling curve, but the reaction temperature determined from the heating curve is closer to the equilibrium temperature.

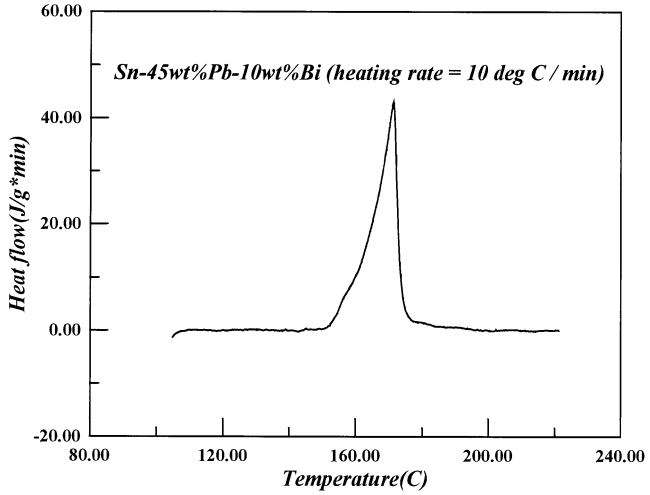

Fig. 6—The DSC heating curve of the Sn-45 wt pct Pb-10 wt pct Bi at the heating rate of 10 °C/min.

The DSC heating curve of the ternary Sn-45 wt pct Pb-10 wt pct Bi alloy is shown in Figure 6. A single large peak is observed, although it is likely that this peak is composed of two smaller peaks. However, not much detail can be resolved. The equilibrium phase relationships of the Bi-Pb-Sn system have been investigated previously,[24,25,26] and there is no report of the existence of any ternary compound. A liquidus projection of the Bi-Pb-Sn ternary system is proposed and is shown in Figure 7, based on the liquidus projection determined by Ho *et al.*[25] and the equilibrium phase diagrams of its three constituent binary systems.[20,21,27] There are four primary solid-phase regions, Bi, $\varepsilon(Bi_3Pb_7)$, Pb, and Sn, in the Bi-Pb-Sn liquidus projection. The cooling curve of the Sn-45 wt pct Pb-10 wt pct Bi alloy at a cooling rate of 10 °C/min is shown in Figure 8, in which three reactions can be observed. The first solid is formed at 176 °C. As indicated in Figure 7, the primary solid phase is Pb. Its solidification path then moves toward the liquidus valley and intersects with the univariant curve (the liquidus valley) at 160 °C, and the Pb and Sn phases solidify simultaneously. The solidification path follows the liquidus valley and passes through the type II reaction, L + Pb =

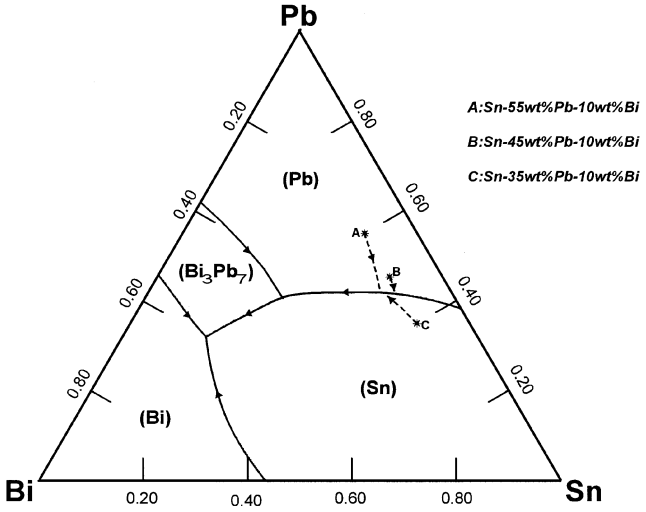

Fig. 7—The solidification paths of the Sn-Pb-Bi alloys superimposed on the liquidus projection of the Sn-Pb-Bi system.

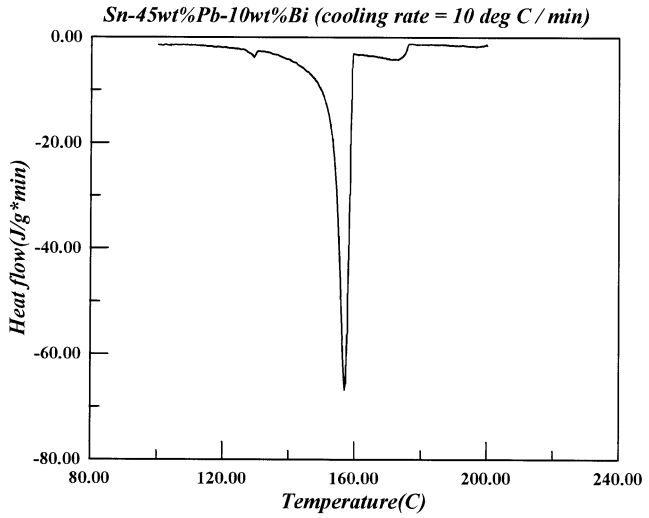

Fig. 8—The DSC cooling curve of the Sn-45 wt pct Pb-10 wt pct Bi at the cooling rate of 10 °C/min.

Bi_3Pb_7 + Sn, at 130 °C. As mentioned previously, the cooling curve is useful in understanding an alloy's solidification mechanisms; however, the undercooling effect is usually not negligible. The temperature of the L + Pb = Bi_3Pb_7 + Sn invariant reaction is 135 °C, based on the heating curves determined in the present DSC study, and is slightly lower than those reported in the literature, which are 137 °C[25] and 138 °C.[26] As shown in Figure 7, the solidification path of the Sn-55 wt pct Pb-10 wt pct Bi alloy is similar to that of the Sn-45 wt pct Pb-10 wt pct Bi, *i.e.*, the primary Pb solid forms first, then the Pb and Sn precipitate simultaneously, and become completely solidified when they encounter the type II reaction. The DSC cooling curve of the Sn-35 wt pct Pb-10 wt pct Bi is shown in Figure 9. Although there are also three reactions shown in Figure 9, the solidification path is different from those of the previous two ternary alloys. As shown in Figure 7, the primary solid for the ternary Sn-35 wt pct Pb-10 wt pct Bi alloy is Sn. The microstructures of the three ternary alloys are shown in Figure 10. The darker phase in Figure 10(a) and (b) is

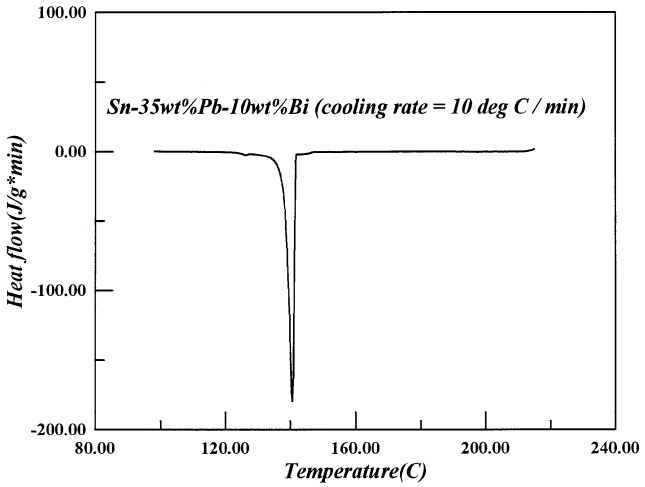

Fig. 9—The DSC cooling curve of the Sn-35 wt pct Pb-10 wt pct Bi at the cooling rate of 10 °C/min.

the primary Pb, and the brighter one in Figure 10(c) is the primary Sn.

A solidification curve, which is a plot of the solid fraction *vs* temperature in the solidification process, is one of the important solidification characteristics of alloys. Although not as straightforward, the solidification curve can also be determined from the DSC experiment. As mentioned previously, various techniques can be used for its determination. A mathematical model for analyzing DSC curves based on the heat-transfer model proposed by Gray[19] has been illustrated in the previous section. Equation [4c] can be used to determine the relationship between the enthalpy release rate ($\Delta h/\Delta t$) with the solidification temperature of the alloy (T), and that between the total enthalpy release (Δh) with T as well. As shown in Figure 8, the first primary solid of the Sn-45 wt pct Pb-10 wt pct Bi melt formed at 176 °C, the semisolid alloy encountered the invariant reaction at 130 °C, and became completely solid at 128 °C. The initial conditions of the numerical solution of Eq. [4c] are that at the beginning of solidification, $t = 0$, $T = 176$ °C, and the total enthalpy release of the melt and the solid fraction are zero. The boundary conditions are that at the end of the solidification, $T = 128$ °C, the total enthalpy release is equal to that of the heat of fusion, 40.5 J/g, and the solid fraction is 100 pct. The information on the heat-flow rate difference ($\Delta q/\Delta t$) *vs* reaction time t is available through the determined DSC cooling curve ($\Delta q/T$) (Figure 8) and the given cooling rate, $\Delta T/\Delta t = 10$ °C/min. Based on the boundary condition that at the end of solidification at 128 °C the total enthalpy release is equal to 40.5 J/g, and using an iteration procedure, the value of R_SC_S can be determined; 0.506945 min. It is further assumed that the amount of heat evolution is directly proportional to the amount of solidified fraction of the melt, and the solidification curve can thus be calculated (Figure 11). Three different regions are observed in Figure 11. The solidification rate of the primary solid in the beginning is relatively slow compared with that of the subsequent simultaneous solidification of Pb and Sn, and the solidification rate decreases sharply toward the end of solidification process. The solidification curves of the Sn-55 wt pct Pb-10 wt pct Bi and Sn-35 wt pct Pb-10 wt pct Bi alloys are also calculated and

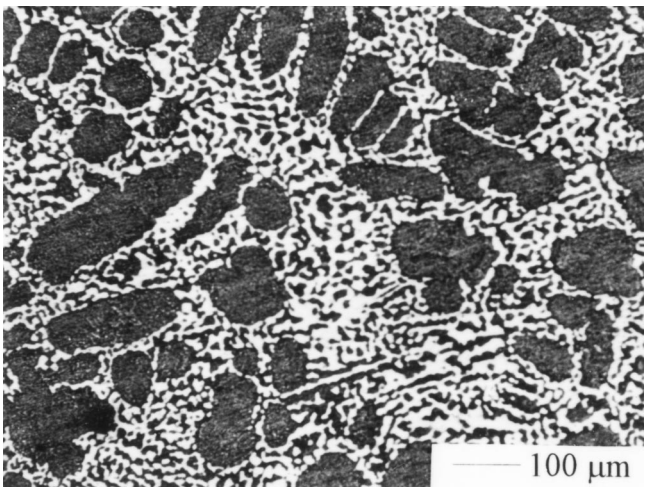

(*a*)

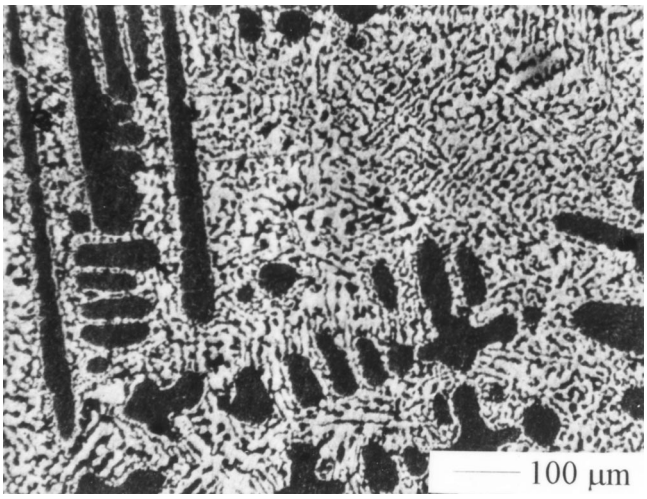

(*b*)

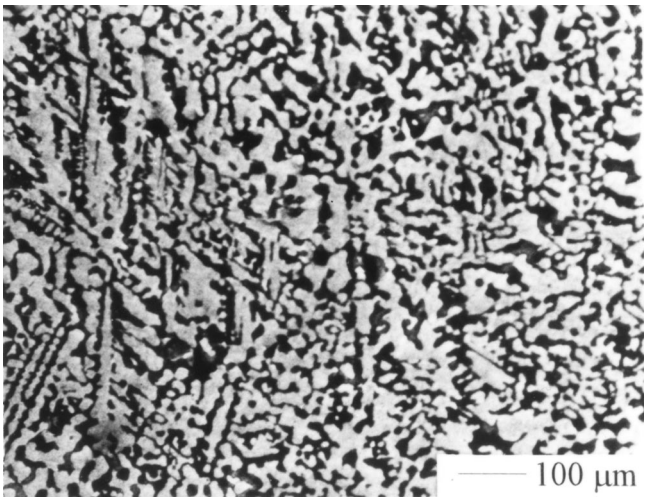

(*c*)

Fig. 10—The microstructures of the (*a*) Sn-55 wt pct Pb-10 wt pct Bi, (*b*) Sn-45 wt pct Pb-10 wt pct Bi, and (*c*) Sn-35 wt pct Pb-10 wt pct Bi alloys.

are shown in Figures 12 and 13, respectively. The curve shapes of the ternary alloys investigated in the present study are all similar and display three regions of different solidification rates.

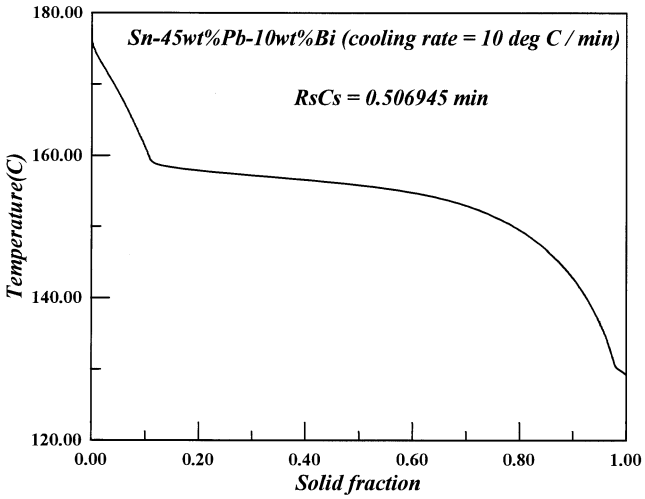

Fig. 11—The solidification curve of the Sn-45 wt pct Pb-10 wt pct Bi alloy.

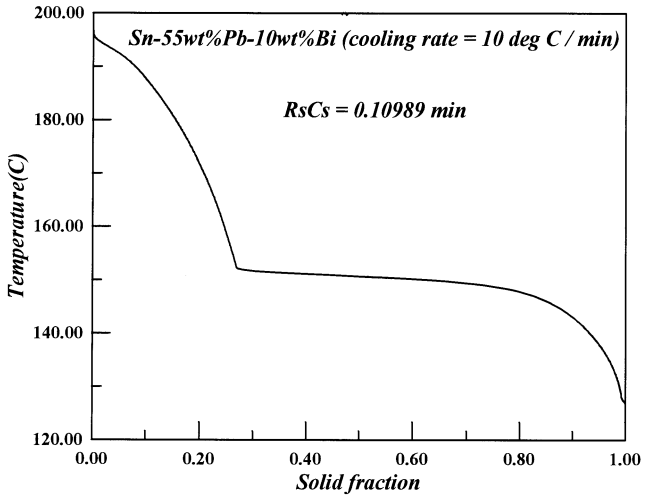

Fig. 12—The solidification curve of the Sn-55 wt pct Pb-10 wt pct Bi alloy.

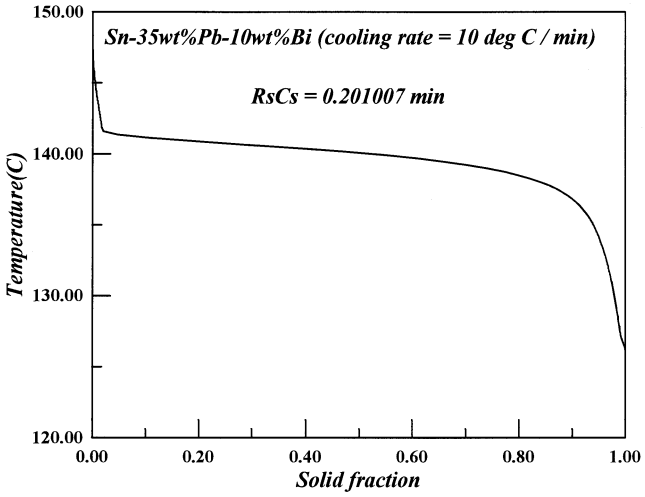

Fig. 13—The solidification curve of the Sn-35 wt pct Pb-10 wt pct Bi alloy.

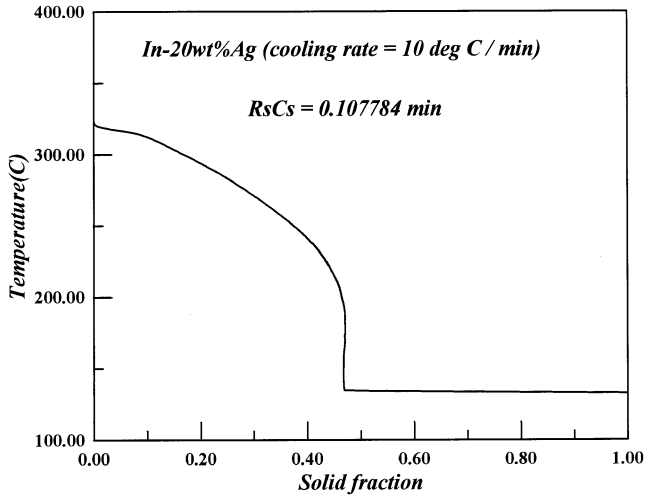

Fig. 14—The solidification curve of the In-20 wt pct Ag alloy.

The solidification curves of the binary alloys are calculated as well. As shown in Figure 14, two different regions can be found in the solidification curves of the In-20 wt pct Ag alloy. The region from 323 °C to 136 °C is associated with the precipitation of the ζ phase, whereas the second part corresponds to the eutectic reaction. The metatectic and peritectic reactions were not observed in the cooling process. Similar nonequilibrium phenomena were also found in the cooling of Cu-In and Cu-Sn alloys.[28,29] If the peritectic and metatectic reactions of the Ag-In system are assumed to be suppressed, the amount of eutectic in the In-20 wt pct Ag alloy is 65 pct, according to the lever rule. The amount of eutectic is 39 pct if an equilibrium condition is assumed. The amount of eutectic in the In-20 wt pct Ag alloy determined from the DSC cooling curve is 47 pct (Figure 14). In most of the solidification processes, the equilibrium condition cannot be obtained and the amount of eutectic is higher than that predicted using the lever rule.[8,30] Although the peaks in the DSC cooling scan, which correspond to the peritectic and metatectic reactions, are absent, the fact that the amount of eutectic is 47 pct which is lower than 65 pct, indicates that these two reactions are not completely suppressed.

V. CONCLUSIONS

Similar to conventional applications, the phase-transformation temperatures and the enthalpies of fusion of the Sn-Pb, Sn-Bi, Ag-Sn, In-Ag, and Sn-Pb-Bi solder alloys have been determined using DSC. Very notable undercooling can be observed in the solidification process of most solder alloys; however, superheating effect is not significant in the heating process. Along with this directly measured information, the solidification curves of various solder alloys have been successfully calculated from the DSC cooling curves based on the mathematical description of heat transfer in the DSC. The solidification curves of alloys are difficult to obtain by other methods.

ACKNOWLEDGMENT

The authors acknowledge the financial support of the National Science Council of Taiwan, Republic of China, through Grant No. NSC 86-2745-E-007-005R.

REFERENCES

1. R.J. Klein Wassink: *Soldering in Electronics*, 2nd ed., Electrochemical Publications, British Isles, 1989.
2. R. Strauss: *Surface Mount Technology*, Butterworth-Heinemann, Oxford, United Kingdom, 1994.
3. H.D. Brody and M.C. Flemings: *Trans. TMS-AIME*, 1996, vol. 236, pp. 615-24.
4. R.J. Claxton: *J. Met.*, 1975, vol. 27 (2), pp. 14-16.
5. G. Fortina and A. Anselmi: *Aluminio*, 1979, vol. 48 (4), pp. 179-87.
6. L. Backerud, E. Krol, and J. Tamminen: *Solidification Characteristics of Aluminum Alloys, Vol. 1: Wrought Alloys*, Skan Aluminum, Oslo, Norway, 1986.
7. A. Roosz and H.E. Exner: *Acta Metall. Mater.*, 1990, vol. 38 (2), pp. 375-80.
8. S.-W. Chen, Y.-Y. Chuang, Y.A. Chang, and M.G. Chu: *Metall. Trans. A*, 1991, vol. 22A, pp. 2837-48.
9. S.-W. Chen and C.-C. Huang: *Acta Mater.*, 1996, vol. 44 (5), pp. 1955-65.
10. S.-W. Chen and S.-C. Jeng: *Metall. Mater. Trans. A*, 1996, vol. 27A, pp. 2722-26.
11. S.-W. Chen and S.-C. Jeng: *Metall. Mater. Trans. A*, 1997, vol. 28A, pp. 503-04.
12. B. Cantor: *J. Thermal Analysis*, 1994, vol. 42, pp. 647-65.
13. P.T. Vianco and D.R. Frear: *JOM*, 1993, vol. 45 (7), pp. 14-19.
14. C. Melton: *JOM*, 1993, pp. 33-35.
15. J. Glazer: *Int. Mater. Rev.*, 1995, vol. 40 (2), pp. 65-93.
16. D.R. Frear: *JOM*, 1996, vol. 48 (5), pp. 49-53.
17. M.T. McCormack, Y. Degani, H.S. Chen, and W.R. Gesick: *JOM*, 1996, pp. 54-56.
18. H. Berg, G. Ganesan, and G. Lewis: *Adv. Packaging*, 1996, vol. 5 (3), pp. 18-22.
19. A.P. Gray: in *Analytical Calorimetry*, R.S. Porter and J.F. Johnson, eds., Plenum Press, New York, NY, 1968, pp. 209-18.
20. I. Karakaya and W.T. Thompson: in *ASM Handbook*, vol. 3, *Alloy Phase Digrams*, H. Baker, ed., ASM INTERNATIONAL, Materials Park, OH, 1992, p. 2.335.
21. H. Okamoto: in *ASM Handbook*, vol. 3, *Alloy Phase Diagrams*, H. Baker, ed., ASM INTERNATIONAL, Materials Park, OH, 1992, p. 2.106.
22. I. Karakaya and W.T. Thompson: in *ASM Handbook*, vol. 3, *Alloy Phase Diagrams*, H. Baker, ed., ASM INTERNATIONAL, Materials Park, OH, 1992, p. 2.37.
23. M.R. Baren: in *ASM Handbook*, vol. 3, *Alloy Phase Diagrams*, H. Baker, ed., ASM INTERNATIONAL, Materials Park, OH, 1992, p. 2.31.
24. E. Janecke: *Z. Metall*. 1937, vol. 29 (11), pp. 367-73.
25. T.-H. Ho, W. Hofmann, and H. Hannemann: *Z. Metall*. 1953, vol. 44, pp. 127-29.
26. R.B. Gershman: *Zh. Fiz. Kh., Moscow*, 1958, vol. 32 (1), pp. 12-18.
27. N.A. Gokcen: in *ASM Handbook*, vol. 3, *Alloy Phase Digrams*, H. Baker, ed., ASM INTERNATIONAL, Materials Park, OH, 1992, p. 2.103.
28. A. Bolcavage, S.-W. Chen, C.R. Kao, Y.A. Chang, and A.D. Romig, Jr: *J. Phase Equilibria*, 1993, vol. 14 (1), pp. 14-21.
29. V.C. Marcotte: IBM East Fishkill, New York, private communication, 1990.
30. S.-W. Chen and Y.A. Chang: *Metall. Trans. A*, 1991, vol. 22A, pp. 267-71.